SLAC-PUB-11070

# Intermediate Strength Gravitational Lensing

J. Irwin, M. Shmakova
*SLAC, Stanford, CA 94025, USA*

Weak lensing is found in the correlations of shear in $10^4$ galaxy images, strong lensing is detected by the obvious distortion of a single galaxy image, whereas intermediate lensing requires detection of less obvious curvature in several neighboring galaxies. Small impact-parameter lensing causes a sextupole distortion whose orientation is correlated with the quadrupole distortion (shear). By looking within a field for the spatial correlation of this sextupole-quadrupole correlation, an intermediate lensing regime is observed. This technique requires correction for the sextupole as well as the quadrupole content of the PSF. We remove the HST PSF and uncover intermediate lensing in the Hubble deep fields. Correlations of the type expected are found.

## 1. Introduction

The traditional weak gravitational lensing techniques [1–3], which locate and quantify the large clumps of matter such as clusters of galaxies (visible or dark) with $10^{14}\,M_\odot$, are not sensitive to the small scale structure or substructure of large clusters. We present here a new method designed to expose small scale structure [4]. We have applied the method to the north Hubble deep field and have seen a signal which has the features expected. We also call this "multipole lensing", since it involves the measurement of the quadrupole and sextupole lensing strengths, and may be extended to other multipoles as well.

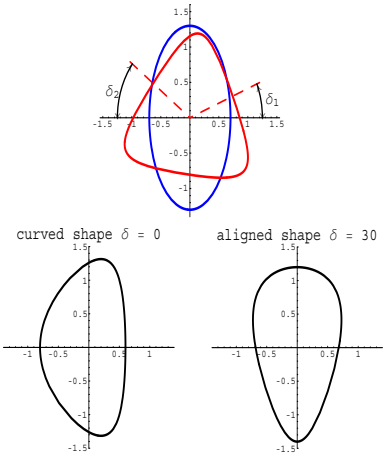


Figure 1: "Curved" and "Aligned" galaxies. $\delta = \delta_1$ if $|\delta_1| < 30°$, else $\delta = \delta_2$. $-30° \le \delta \le 30°$, where $\delta \sim 0°$ for "curved" and $\delta \sim \pm 30°$ for "aligned" galaxies.

## 2. General lensing kicks and maps

This power series expansion from the $1/r$ deflection of a light stream by a point mass can be generalized to yield the kick in both coordinates:

$$\Delta x' + i\Delta y' = -\frac{4MG}{x_0 + (\Delta x - i\Delta y)} \qquad (1)$$
$$= -\frac{4MG}{x_0}\left[1 - \frac{\Delta x - i\Delta y}{x_0} + \left(\frac{\Delta x - i\Delta y}{x_0}\right)^2 + ...\right].$$

Concentrating on the linear term, one sees for example that the horizontal kick is de-focusing, while the vertical kick is focusing. The image appears larger in the focused direction and smaller in the de-focused direction, hence the linear term changes a circle into an ellipse. It is a general feature that the image distortions have the opposite sign of the map coefficients. The 2nd-order term is the sextupole term. For $\Delta y = 0$, $\Delta x > 0$ the deflections of the 1st- and 2nd-order terms have the opposite sign, hence the quadrupole is minimum there and the sextupole term is maximum. For $\Delta y = 0$, $\Delta x < 0$ the quadrupole has its other minimum and the sextupole also has a minimum. Below in the lower group of fig. 1 are shown the superposition of quadrupole and sextupole distortions for two distinct orientations of the sextupole moment with respect to the quadrupole moment. It is the curved shape that would arise from a lensing event.

The plan we will follow is to measure the quadrupole and sextupole shape of all galaxies, classify each galaxy according to whether it is "curved", "mid-range" or "aligned", and examine the distribution of "curved" galaxies on the sky to determine if curved galaxies are randomly distributed or unusually clumped.

The lensing map can be written as a set of 4 functions $x_S(x_T, y_T)$, $y_S(x_T, y_T)$, $x'_S(x_T, y_T)$, and $y'_S(x_T, y_T)$, where "T" designates "telescope" and "S" designates "source". The two functions $x_S(x_T, y_T)$ and $y_S(x_T, y_T)$ can be combined into one complex function by defining $w_S = x_S + iy_S$. Since the transverse width of the light stream will be small compared to characteristic dimensions of the variations of the lensing mass distributions, we may expand this


*Presented at 22nd Texas Symposium On Relativistic Astrophysics, 12/13/2004-12/17/2004, Stanford, CA, USA*
Work supported in part by the Department of Energy contract DE-AC02-76SF00515

function in a power series about the stream centroid:

$$w_S(w_T, \bar{w}_T) = w_T + \sum_{n,m=0}^{\infty} a_{nm} w_T^n \bar{w}_T^m. \qquad (2)$$

The significance of the variables $w$ and $\bar{w}$ rests on the fact that products and powers of them are rotation eigenfunctions. It follows that the terms in the expansion for $w_S$ have a simple interpretation. The $1 + a_{10}$ combination represents a simple rotation and scaling, the $a_{01}$ term is a quadrupolar distortion (connected to shear in weak lensing) , the $a_{02}$ term is a sextupolar distortion, the $a_{03}$ term is an octupolar distortion, the $a_{20}$ term is a cardioid-like distortion, and the $a_{11}$ term is an $r^2$-dependent translation of circles, and so on. We will be concerned primarily with the terms $a_{01}$, $a_{02}$ and refer to them more simply by the letters, $a$ and $b$, respectively.

In accord with the variables chosen for the map, we expand the solution to Laplace's equation in the variables $w = x + iy$ and $\bar{w} = x - iy$. Variables without subscripts are taken to lie in the lensing plane. Using these variables, the power series expansion for the potential is $\Phi = \sum_{n,m=0}^{\infty} \frac{1}{n!m!} \Phi_{nm} w^n \bar{w}^m$ where $\Phi_{nm} = \partial^n \bar{\partial}^m \Phi$ evaluated at $w = w_0$. If both $n$ and $m$ are greater than or equal to 1, the term will be proportional to the density or a derivative of the density, since $\Phi_{11} = \frac{1}{4}\nabla^2\Phi = \pi G\rho$. The two components of the kick, given in the form $\Delta x' + i\Delta y'$, are contained in the single equation,

$$\Delta w' = -2\,\bar{\partial}(2\Phi). \qquad (3)$$

The geometry of the deflection implies that $w_S = w_T + D_{LS}\Delta w'(w, \bar{w})$ with $w = \frac{D_{TL}}{D_{TS}} w_T$, where $D_{LS}, D_{LT}$ and $D_{TS}$ are comoving distances from the lensing plane to the source, from the lensing plane to the telescope, and from the telescope to the source, respectively, divided by $1 + z_L$, with $z_L$ is the redshift of the lensing plane. Thus for a general potential the map coefficients are given by

$$\begin{aligned} a_{10} &= -4D_{LS}\frac{D_{TL}}{D_{TS}}\Phi_{11} = -4\pi G D_{LS}\frac{D_{TL}}{D_{TS}}\rho, \\ a &= -4D_{LS}\frac{D_{TL}}{D_{TS}}\Phi_{02}, \\ b &= -4D_{LS}\left(\frac{D_{TL}}{D_{TS}}\right)^2 \frac{1}{2}\Phi_{03}. \end{aligned} \qquad (4)$$

The map coefficients for the point source may be found by evaluating the derivatives of $2\Phi_\delta = 4MG\,Ln\,[r] = 2MG\,Ln\,[w\bar{w}]$:

$$\begin{aligned} a_\delta &= D_{LS}\frac{D_{TL}}{D_{TS}}\frac{4MG}{\bar{w}_0^2}, \\ b_\delta &= -D_{LS}\left(\frac{D_{TL}}{D_{TS}}\right)^2 \frac{4MG}{\bar{w}_0^3}. \end{aligned} \qquad (5)$$

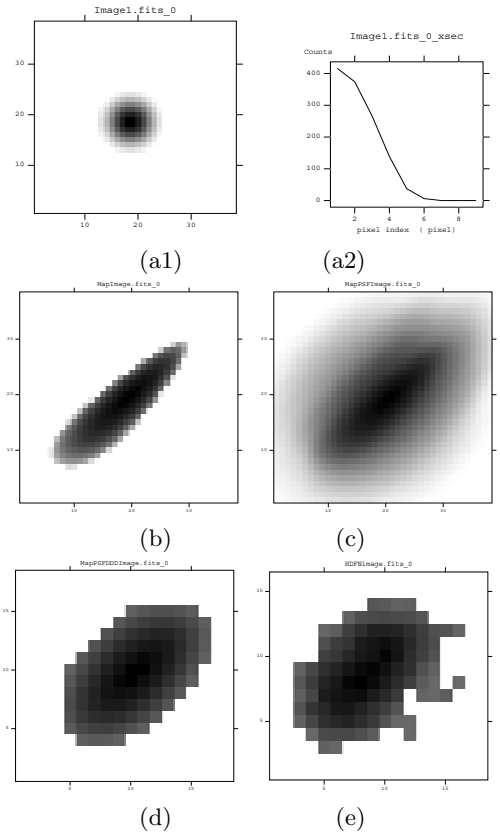


Figure 2: Schematic presentation for the model method. The initial azimuthally symmetric image (a1) with radial profile (a2), get distorted by a lensing with $a$ and $b$ map coefficients (b) and smeared by HDF PSF (c). The graph (d) is a final simulated image after application of charge diffusion, dithering and drizzle. The image (e) is a real HDF galaxy those distortion has been identified by the "Model" method.

## 3. Model method to determine map coefficients

We use a novel method to estimate lensing map coefficients that takes into account the point-spread function (PSF), the diffusion of charge between camera pixels, the dithering of pointing, and drizzle of photon counts onto the final pixel grid.

The standard "moment" [5] method has the advantage of simplicity, but because the images are necessarily truncated its accuracy is compromised as a result of edge effects and an inherent ambiguity in including the effect of the PSF. Furthermore, it does not bring into play the knowledge that moments derived from the action of lensing will have a radial strength proportional to the derivative of the radial profile of the galaxy. The radial-fit method overcomes these shortcomings. The model method begins with a parameterized radial profile of the source galaxy and in addition models the PSF, diffusion and other image composition processes (see fig. 2). This latter method

is limited by the imperfect knowledge of the features it seeks to include (such as PSF and charge diffusion), plus of course, the noise inherent in background galaxy shapes and photon counting noise. Background galaxies can have shapes that mimic lensing, one can show in this case that this method gives a vectorial sum of the lensing coefficient and the background value.

We assume a radial profile for the background galaxy of the form [1]

$$F(r_S^2) = c_0(A + B(\frac{r_S}{r_0})^2 + C(\frac{r_S}{r_0})^4)_+ \, e^{-D(\frac{r_S}{r_0})^2}, \quad (6)$$

This function must depend only on $r_S^2$. The parameter $r_0$ is taken to be near the rms size of the source image. By changing the size of $r_0$ one can change the size of the image without affecting its shape. The factor $c_0$ is introduced so that the shape parameters, which are dimensionless, have values $A \approx 1$ and $B$ and $C$ can be compared to unity. The + subscript indicates that if the polynomial has a value less than zero, it is to be set equal to zero.

The effect of lensing is contained in the parameters of the map of eq. 2. One replaces each occurrence of $r_S^2$ by the expression $w_S \bar{w}_S$.

The parameters of the radial profile and the map are determined by minimizing the L2 norm:

$$\|i_F - i_T\|_\rho^2 = \int (i_F - i_T)^2 \, \rho \, dx_T dy_T \quad (7)$$

where $i_F = F(r_S^2)\,|\frac{\partial w_S}{\partial w_T}|$. $i_T$ is the light-intensity function normalized to unit integral and according to the notation introduced in the previous section the subscript $T$ means the intensity as observed at the telescope. In $i_F$, $r_S^2 = w_S \bar{w}_S$ is understood to be a function of $x_T$ and $y_T$ through $w_T$ and $\bar{w}_T$. The $|...|$ is the Jacobian of the transformation between $S$ and $T$ variables. All map variables in the Jacobian occur in 2nd order except for the $d$ variable, which occurs in 1st order. A weight function $\rho$ can be introduced if desired. However, because this technique ignores truncated pixels rather than considering them to be zero, edge effects are inherently smaller compared to the moment method. At each calculation of $i_F$ the Jacobian is monitored to see that it is not negative at that or any smaller $r$.

The model method begins by constructing an $i_F$ (here on .02" pixels) (fig. 2(b)) and convolving it with a sub-sampled PSF (also on .02" pixels) as provided by the Tiny Tim program (fig. 2(c)). This convolved image is dropped (25 times) onto a dithered original pixel grid (0.1" pixels). A diffusion kernel is applied to each resulting image. The image on each original pixel is shrunk to half its size in each dimension, and then "drizzled" to the final Hubble deep field grid (0.04" pixels) according to the intersection of the diminished original pixel area with the pixels in the final grid (fig. 2(d)).

## 4. Sextupole-quadrupole measurements and relative orientation

The software SExtractor [7] was used to select galaxies from the Hubble deep field and to specify which pixels to include in the image. Galaxies were selected which appeared for both a $4\sigma_{NF}$ and a $6\sigma_{NF}$ threshold option (4 or 6 times the rms noise floor) with the convolution option taken to be the identity. Only galaxies that had been assigned a $z$-value with $z > 0.8$ were kept. [2] There were about 569 galaxies so identified in the north field. The images used in our analysis were cut at $6\sigma_{NF}$ and defined to be the dominant simply-connected region.

Galaxy images were transferred to the *Mathematica* programming environment for inspection where galaxies with more than one maxima were removed. Of the 569 identified galaxies with $z > 0.8$, 427 survived this single-max cut.

We have also impose the noise cuts based on Poisson-noise estimation [8]. The following list summarizes the results on the several galaxy cuts:

| | |
|---|---|
| 569 | in the z-catalog with $z > 0.8$ and found by SExtractor for thresholds $4\sigma_{NF}$ and $6\sigma_{NF}$; |
| 427 | having only one prominent maximum; |
| 370 | larger than 5 pixels in both x and y; |
| 323 | with radial-fit having its L2 squared norm less than 0.05 ("good fit" condition); |
| 217 | satisfying the signal-to-noise cut condition described in [8]. |

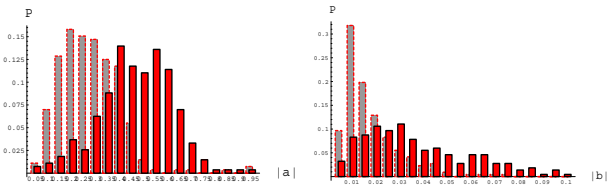


Figure 3: Distribution of the magnitude of the quadrupole map coefficients (left plot) and sextupole map coefficient (right plot), using the model method (foreground) compared with the fit method (background).The units of sextupole coefficients are "per HDF pixel".

[1] K. Kuijken [6] introduced the radial-fit method, taking a sum of Gaussians as the ansatz for the radial profile.

[2] We used z-catalogs from ess.sunysb.edu/astro/hdf.html and bat.phys.unsw.edu.au/ fsoto/hdfcat.html.

In fig. 3 we show the distribution of magnitude of the quadrupole coefficient (left) and the distribution of sextupole coefficients (right) that were found by radial-fit (background) method and model method (foreground).

The orientation of the sextupole map coefficient with respect to the quadrupole coefficient is of primary interest to us. A plot of the (smallest) angle between sextupole and quadrupole minima using the model method is shown in fig. 4 for the galaxies surviving both the L2 norm $< 0.05$ cut and the signal-to-noise cut. This angle, which we refer to as $\delta$, runs from $0°$ to $30°$. For $\delta = 30°$ the shapes will have aligned maxima, and we refer to such galaxies as "aligned". They are pear shaped galaxies, as compared to the "curved" galaxies which resemble bananas. See fig. 1. Figure 5 compares $\delta$ found with the radial-fit and

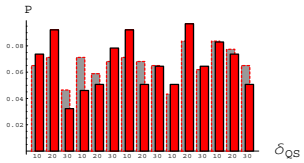


Figure 4: The distribuiton of the magnitude of $\delta$, the smallest angle between a quadrupole minimum and a sextupole minimum, using the model method, for galaxies in the north HDF after the noise cut and all galaxies surviving the L2 cut (background).

model methods. We now proceed to a study of the

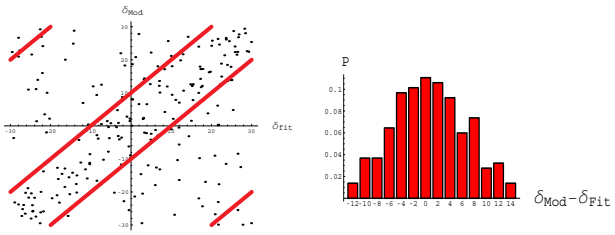


Figure 5: The left panel compares the angle $\delta$ as measured by the radial-fit method and the model method. The points within the diagonal band (or in the corners) have a change in $\delta < 10°$ . The distribution for $\delta_{Mod} - \delta_{Fit}$ is shown on the right panel.

spatial distributions of the "curved" and "aligned" galaxies as determined in this section.

## 5. Clumping of curved galaxies

To quantify clumping for a galaxy subset with $N_C$ members, we draw a circle of fixed radius $R$ about each member of the subset and count the members of that subset which lie within the circle. We then compare the distribution of the number of galaxies having 0, 1, 2, 3, etc. neighbors closer than $R$, with a large number of such distributions derived from randomly chosen subsets having the same number ($N_C$) of galaxies in two distinct ways:
(1) for an informative but qualitative comparison, we compare the distribution of the initial subset with the average distribution of the random subsets, and
(2) for a quantitative comparison, for the subset being studied and for each of 500 randomly selected subsets having the same number of galaxies as the original subset, we sum the galaxies having $N$ or more neighbors (usually $N = 4$). Each random subset is thereby associated with a single number, $n_G$, the number of galaxies of that subset having $N$ or more neighbors. We then create a bar graph, showing for each value for $n_G$ the number of random subsets which had that number of galaxies with $N$ or more neighbors. This distribution is thus a property of random subsets of a size $N_C$, with neighbor distance $R$, for the specified neighbor range. Since the initial subset will have a certain number, $n_G$, of galaxies having $N$ or more neighbors, we can ask the question "what fraction of randomly chosen galaxy subsets have that many or more members with $N$ or more neighbors?" We thereby determine a probability that this configuration could occur by chance.

For "curved" galaxies we begin with bar graphs of type 1 comparing the neighbor distribution with the average of randomly chosen subsets. In fig. 6 (a), we show the distribution of the number of neighbors in a circle of radius $R = 280$ [3] for the "curved" galaxies using the model method (which we now take to be $\delta < 9°$.) Fig. 6 (b) displays an analysis of type 2 for

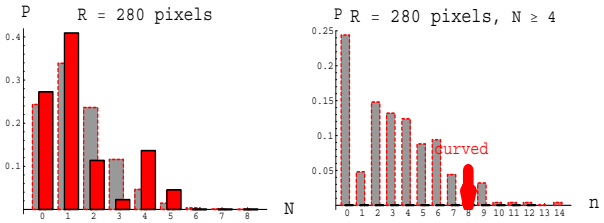


(a) (b)

Figure 6: A histogram showing the fraction of curved galaxies having a specific number, N, of curved neighbors within a circle of radius 280 pixels, compared with the average of such a distribution for 500 randomly chosen subsets having the same number of galaxies.

the model method. (The number corresponding to the "curved" set is indicated by an arrow in this bar

[3]The Hubble deep field images have a drizzled pixel size of 0.04 arc sec. At $z$ =0.6 for current cosmological parameters (dark matter 23%, baryons 4%, dark energy 73%) the distance scale would be 6.67 kpc per arc sec. 280 pixels corresponds to 75 kpc.

graph.) For the optimum radius, which is typically between 270 and 340 pixels, there will be less than 25 out of 500 sets that have as many galaxy-circles with counts equal to or greater than the original curved set. In other words, the probability of achieving the curved set by chance is equal to or smaller than 5%.

Figure 7 shows "curved" galaxies (as determined using model method) in the Hubble north field and for galaxies having three or more neighbors, their neighborhood circles of radius R=280 pixels. Large "stars" indicate "curved" galaxies, and small "stars" indicate remaining background galaxies.

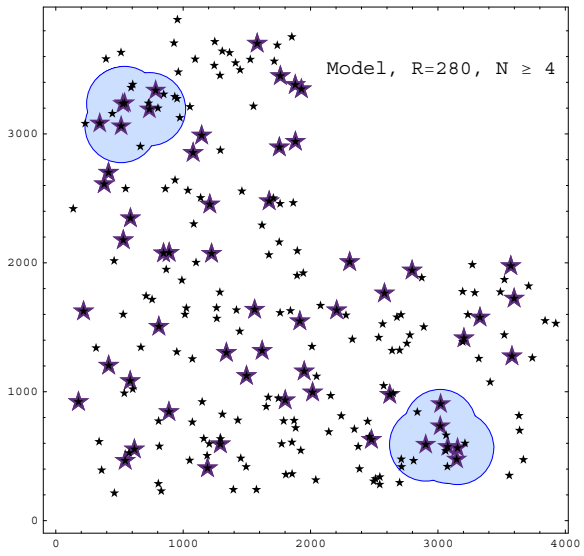


Figure 7: A field plot showing the spatial location of "curved" galaxies in the north HDF using the model method to determine the map coefficients. Large "stars" indicate "curved" galaxies and small "stars" indicate the remaining background galaxies that survived the joint-variable signal-to-noise cut. Circles are shown for 4 or more neighbors.

Significantly these results improve as noise constraints are relaxed. In this case the clumping signal becomes stronger with the random probability decreasing from 5% to 2.5%. Furthermore if the z-distributions of the random sets are constrained to resemble the distributions of curved galaxies the probability decreases to 1.5%.

Given any background distribution of orientations between sextupole and quadrupole moments, lensing events will statistically move a galaxy to a "more curved" condition. Since there is a lot of mass at distances where the quadrupole and/or the sextupole deflection coefficient is small there could arise many weaker "nudges" toward a "more-curved" condition. Thus the "aligned" galaxies will be depleted in a non-uniform way. For this reason we now apply the previous analysis of "curved" galaxies to "aligned galaxies". Similar to the above analysis gives 8%-10% probability for the aligne galaxies to be clumped for a larger radius of the group $R \sim 340$ pixels.

## 6. Total lensing-mass requirements

To simplify our considerations we assume that 1) the observed increase in the number of galaxies with 4 or more neighbors comes from the addition of 1 or 2 lensing mass "overdensities", 2) the constituent halo masses can be taken to have a single value, and 3) the spatial distribution of this constituent can be sufficiently-well approximated by a top-hat distribution. The lensing mass is assumed to lie in the region $0.3 < z < 1.25$ where the geometrical coefficients for lensing are large. We project any lensing mass that exists in this region onto a lensing plane at z=0.6.

The probability to have a scattering event must be substantial where clumping is seen. An area of $\pi 280^2$ pixels would typically contain 9 background galaxies. Assuming the they are equally divided between curved, mid-range and aligned, then to get a final total of 5 curved, of the 6 originally non-curved background galaxies at least 2 must get curved. So the probability for a background galaxy to be lensed by a sufficiently strong small-impact parameter lensing event must be near 33%.

For a top-hat distribution of constituents having a single mass, the total mass in the distribution will be

$$M_X G = \rho G\, A_X = \frac{MG}{d_X^2} A_X = \frac{MG}{r_0^2}\frac{r_0^2}{d_X^2} A_X \quad (8)$$
$$= \frac{1}{4\pi}\frac{D_{TS} D_{TL}}{D_{LS}}\, a_{typ}\, P_a \mathcal{A}_{\mathcal{X}},$$

where $\rho$ is the (projected) density of the constituents, $A_X$ is the area of the overdensity, $M$ is the mass of the constituent clumps, and $d_X$ is a characteristic cell size or projected separation distance of the haloes within the overdensity. $r_0^2$, the square of a typical impact parameter, is chosen so that when $M/r_0^2$ is inserted in the formula for $a$, one finds a typical induced quadrupole coefficient for those events that transform the local galaxy light-streams to the curved shape. $P_a \equiv \pi r_0^2/d_X^2$, which is the ratio of the typical impact parameter area to the cell size, can be interpreted as the probability that any particular light path receive an induced map coefficient change of the observed and required magnitude. $\mathcal{A}_{\mathcal{X}}$ is the area of the group in square radians. The observed clumps have areas of $\pi 280^2 \approx 2.5\, 10^5$ square pixels.

As noted above, the probability to be transformed from not-curved to curved must be the order of 33%. We suppose that for any particular galaxy the transformation from not-curved to curved depends on the probability that the background galaxy is suitable (for example its moments are small enough to easily alter or their orientation is conducive to change) times the

probability that the kick is large enough. We assume that these probabilities are roughly equal, and hence get a probability of $P_a \approx 0.6$ that the kick is large enough. ($P_a \approx 0.6$ implies $d_X/r_0 \approx 2.3$.)

The typical quadrupole lensing coefficient, $a_{typ}$, for these events has to be large enough to change moment alignments, so it must be comparable to but can probably be less than the average of the background coefficients, which can be estimated to be a bit less than $< a >$, as deduced from the model method, because we have already included a factor to insure that the background galaxy is "suitable" . For $a_{typ} \approx 0.2$, $P_a \approx 0.6$, $\mathcal{A}_{\mathcal{X}} = 10^{-8}$ square radians (corresponding to $2.5\,10^5$ square pixels), and setting $D_{TL} = D_{LS} = 1.4$ Gpc for a lensing plane at $z = 0.6$, we find $M_X G \approx 0.27\ pc \Leftrightarrow M_X = 5.6\,10^{12}\ M_\odot$.

This estimate depends on: the area of the region of enhanced "curving", the enhancement of the probability of finding a curved galaxy in that region, and the typical value of the quadrupole map coefficient. While these numbers can vary somewhat, each is confined to a narrow range.

We have also simulated this situation, randomizing the position of the background galaxies, randomizing background values of map coefficients according to our measurements, and randomizing overdensity constituent positions. The result is that to identify an overdensity 50% of the time requires a total lensing mass of $5\,10^{12} M_\odot$.

## 7. Probable overdensity origins

Using 0.27 times the critical density one finds that the average matter behind a circle of radius 280 pixels in the region from $0.3 < z < 1.25$ has a mass of $6.8\,10^{12} M_\odot$. But only constituents with a mass $10^9 < M < 5\,10^{11} M_\odot$ can be seen. Smaller masses require an impact parameter smaller than the background galaxy radii. Larger masses have radii that are too large to achieve the required impact parameters. See fig. 8. One can use the Sheth-Tormen [9] distribution to estimate the fraction of the total mass with halo mass in this mass range to be about $1/5^{th}$, which equals $1.4\,10^{12} M_\odot$. There is actually a bit more detectable mass than this, because the large haloes have large radii, so that light paths will be penetrating them and can detect sub-structure they might contain. We estimate this sub-halo mass at $0.3\,10^{12} M_\odot$, achieving a grand total estimate of an average total mass in the detectable constituent mass range of $1.7\,10^{12} M_\odot$.

To estimate the overdensity and underdensity extremes we looked at the visible haloes between $0.3 < z < 1.25$. One finds that in areas of radius 280 pixels, the overdensities reach twice their average and the underdensities go to zero. So if the invisible mass is organized according to the visible mass, one would

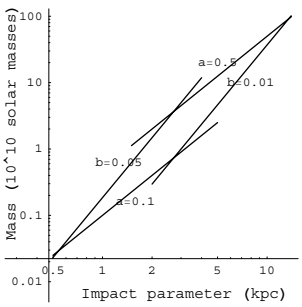


Figure 8: A plot of the constituent mass versus the impact parameter. Lines of constant $a$ and $b$ are shown which delineate the range of $a$ and $b$ observed. The range of values using the model method are shown. The lensing plane is taken to lie at $z = 0.6$.

expect an overdensity of $3.4\,10^{12} M_\odot$. This is close to the lensing-based estimate of $5\,10^{12} M_\odot$. More convincingly the maximum overdensity of visible haloes is coincident with the the clump of curved galaxies in the upper left of the field in fig. 7.

We do not judge the discrepancy between our estimates of the lensing mass and overdensity mass to be significant. Since the process is statistical, a range of overdensities can produce the clumping of lensing curvature we observe. But we would venture, that in larger fields with more statistics, observations could begin to constrain halo distribution models.

## Acknowledgments

Work supported by Department of Energy contract DE-AC03-76SF00515.

## References

[1] H. Hoekstra, H. Yee and M. Gladders, New Astron. Rev. **46**, 767 (2002) [arXiv:astro-ph/0205205].
[2] Y. Mellier, L. van Waerbeke, E. Bertin, I. Tereno and F. Bernardeau, arXiv:astro-ph/0210091.
[3] D. M. Wittman, J. A. Tyson, D. Kirkman, I. Dell'Antonio and G. Bernstein, Nature **405**, 143 (2000).
[4] J. Irwin and M. Shmakova, arXiv:astro-ph/0308007.
[5] N. Kaiser, G. Wilson and G. A. Luppino, arXiv:astro-ph/0003338.
[6] K. Kuijken, arXiv:astro-ph/9904418.
[7] E. Bertin and S. Arnouts, Astron. Astrophys. Suppl. Ser.**117**, 393 (1996)
[8] J. Irwin and M. Shmakova, to be published in the New Astronomy Reviews, Elsevier (2005).

[9] R. K. Sheth and G. Tormen, Mon. Not. Roy. Astron. Soc. **308**, 119 (1999).